sustainability

MDPI

Article

Multi-Objective Optimization of a Hybrid ESS Based on Optimal Energy Management Strategy for LHDs

Jiajun Liu, Tianxu Jin *, Li Liu, Yajue Chen and Kun Yuan

School of Mechanical Engineering, University of Science and Technology Beijing, Beijing 100083, China; b20140331@xs.ustb.edu.cn (J.L.); liliu@ustb.edu.cn (L.L.); s20150427@xs.ustb.edu.cn (Y.C.); b20120359@xs.ustb.edu.cn (K.Y.)

* Correspondence: JTX13810319966@ustb.edu.cn; Tel.: +86-10-8237-5949

Received: 10 September 2017; Accepted: 13 October 2017; Published: 21 October 2017

Abstract: Energy storage systems (ESS) play an important role in the performance of mining vehicles. A hybrid ESS combining both batteries (BTs) and supercapacitors (SCs) is one of the most promising solutions. As a case study, this paper discusses the optimal hybrid ESS sizing and energy management strategy (EMS) of 14-ton underground load-haul-dump vehicles (LHDs). Three novel contributions are added to the relevant literature. First, a multi-objective optimization is formulated regarding energy consumption and the total cost of a hybrid ESS, which are the key factors of LHDs, and a battery capacity degradation model is used. During the process, dynamic programming (DP)-based EMS is employed to obtain the optimal energy consumption and hybrid ESS power profiles. Second, a 10-year life cycle cost model of a hybrid ESS for LHDs is established to calculate the total cost, including capital cost, operating cost, and replacement cost. According to the optimization results, three solutions chosen from the Pareto front are compared comprehensively, and the optimal one is selected. Finally, the optimal and battery-only options are compared quantitatively using the same objectives, and the hybrid ESS is found to be a more economical and efficient option.

Keywords: load-haul-dump vehicle; multi-objective optimization; hybrid energy storage system; energy management strategy; parameter sizing; battery capacity loss

1. Introduction

The underground load-haul-dump vehicles (LHDs) are one of the most commonly used equipment in the mining industry. As their name implies, the vehicles are used to load the ore at the draw points or in the stopes, and to haul it to the ore passes or the mining trucks. However, the LHD is typically driven by a diesel engine. Emissions such as CO_2, NO_X, and particles will cause much damage to the underground environment and human health due to significant energy consumption, a closed working environment, and limited ventilation conditions [1]. With increasing concern about energy conservation and underground environmental protection, a solution must be developed that saves energy and reduces emissions.

The existing alternative is to use an energy storage system (ESS), typically batteries (BTs) or supercapacitors (SCs), to reduce or even achieve zero emissions [2]. There are several ESS technologies applied in the field of mining vehicles [3–9]. Zeng et al. [4] compared the energy saving effects of four different energy management strategies (EMSs) used in a diesel—BT hybrid loader, and selected the most recommended one to guide application. Nilsson et al. [5] presented a predictive EMS based on stochastic dynamic programming (SDP) for diesel—SC hybrid loaders. Simulations and field tests have shown that the proposed controller gives around 5% lower fuel consumption than the nonpredictive one. Unger et al. [8] proposed a real-time model predictive control concept and introduced a data-based methodology to predict the future load demand. A testbed for the diesel–BT hybrid loader was developed to verify the effectiveness of the EMS.

However, all of the aforementioned papers focus only on the EMS of ESS-based mining vehicles, regardless of the sizing problem of powertrain parameters. Much of the literature implies that EMS and parameter sizing always couple with each other in hybrid electric vehicles (HEVs) and electric vehicles (EVs).

Some authors tend to formulate an integrated optimization solving EMS and component sizing simultaneously. Kim et al. [10] suggested a combined framework to optimize power management and the component sizing of fuel cell/battery hybrid vehicles, and achieved excellent fuel economy. Song et al. established an integrated optimization problem using dynamic programming (DP) to minimize the hybrid ESS life cycle cost, and obtained the optimal size of the SC packs in EVs [11]. They also evaluated the influence of different driving cycles on the integrated optimization of hybrid ESS, with the operation cost as the objective, including the SC size and EMS for EVs [12]. Hung et al. [13] developed a combined optimal sizing and EMS for the in-wheel motors of EVs, and used a global search method (GSM) to minimize the power consumed by the battery. Liu et al. [14] developed a power source sizing model, applying Pontryagin's minimum principle (PMP) as the power management strategy, to optimize battery lifetime while reducing battery energy loss, fuel consumption, and powertrain cost. Murgovski et al. [15] gave a novel methodology based on convex optimization to minimize the cost for fuel, electricity, and energy buffer, solving the problem of battery size and EMS for plug-in HEVs (PHEVs). Compared to DP, convex optimization has similar results, and no curse of dimensionality. Using this efficient approach, Hu et al. solved many of these problems, including minimizing the cost of hydrogen and hybrid ESS in a fuel cell HEV (FCHEV) [16], the total amount of daily CO_2 emissions in PHEVs [17], and the hydrogen cost and proton exchange membrane fuel cell power variation in a case study of a FCHEV [18].

Other authors try to establish a multi-objective optimization framework. Xu et al. [19] introduced a two-loop framework of FCEVs to obtain the optimal fuel economy and system durability. Ebbesen et al. [20] evaluated particle swarm optimization (PSO) for solving the optimization problem of sizing the drive-train components; they defined the objective as a weighted sum of fuel consumption and cost of hybridization. Herrera et al. [21] presented an adaptive EMS, based on fuzzy logic, and the optimal sizing for a tramway with BTs and SCs, solved by multi-objective genetic algorithms. The objective function included the costs of the energy absorbed from the catenary, as well as the operation cost of the hybrid ESS. Song et al. [22] proposed a semi-active hybrid ESS topology in EVs, including a novel quantitative battery capacity fade model, and minimized both the cost of the hybrid ESS and the battery capacity loss. Hu et al. [23] proposed a soft-run strategy for a real-time and multi-objective control algorithm design for a FCEV, and achieved a good balance of fuel economy and system durability in a demonstration operation.

Besides, for EMS research, Martinez et al. [24] presented a thorough survey of the latest progress in optimization-based algorithms of PHEVs. Silvas et al. [25] introduced a comprehensive analysis of the various methodologies for system-level design in HEVs. Zhang et al. [26] proposed an equivalent consumption minimization strategy (ECMS) aimed at minimizing the hydrogen consumption for a fuel cell/battery/ultracapacitor tram. Hemi et al. [27] presented an EMS based on PMP and the Markov chain method to minimize the hydrogen consumption for a FCEV. The Markov chain was developed to predict the power. Wieczorek et al. [28] introduced a mathematical representation of an EMS for hybrid ESS in EVs that optimized the energy consumption, and compared the two strategies generated from the method with a rule-based strategy and battery-powered system.

Owing to the huge income in mining industry, productivity is perhaps the most important economic consideration when evaluating the performance of LHDs [1]. In addition, in order to evaluate the feasibility of the design, the total cost should also be given priority. However, the optimization-based algorithms applied to passenger vehicles usually do not consider these key factors at the same time.

To this date, BTs are one of the most widely used ESS in LHDs, and some manufacturers have already released the battery LHD products, such as Atlas Copco [29], RDH Mining Equipment [30,31],

and Artisan Vehicle Systems [32]. BTs on an LHD need to meet the peak and instantaneous power demand. The high and frequent discharge current tends to have a significant impact on battery lifetime, which leads to increase the cost of ESS [33–38]. SCs have an extremely high power density and sufficient durability, but very low energy density. The overall performance could be enhanced by using hybrid ESS that combine the functionalities of BT and SC [39–43]. However, to the author's knowledge, very few papers have been published that focus on evaluating the performance of hybrid ESS in LHDs.

Therefore, this paper, as a case study for hybrid ESS-based LHDs, aims to make three contributions: (1) a multi-objective optimization of the hybrid ESS sizing and EMS, with LHD key factors as optimization objectives, including a battery capacity degradation model; (2) a 10-year life cycle cost model of hybrid ESS for LHDs; and (3) a quantitative performance comparison between the optimal hybrid ESS and battery-only options. This paper is organized as follows: In Section 2, we describe the driving cycle of LHDs and introduce the data applied in this paper. Section 3 proposes the powertrain configuration of a hybrid ESS-based LHD and develops the models of BT packs, SC packs, battery capacity degradation, and other powertrain elements. In Section 4, we formulate a multi-objective optimization framework of parameter sizing based on DP and Pareto optimization, and establish a life cycle cost model of hybrid ESS. Section 5 sets up a comparison between the optimal hybrid ESS and battery-only options. The conclusions are summarized in Section 6.

2. Driving Cycle Description

Figure 1 shows a typical driving cycle of LHDs, which can be divided into six phases, including: towards draw points, bucket loading, leaving draw points, hauling, bucket emptying, and reversing. Starting from point A, the LHD is driving towards the draw points for loading, then hauling to the dumping point B, emptying the bucket and reversing back to point A.

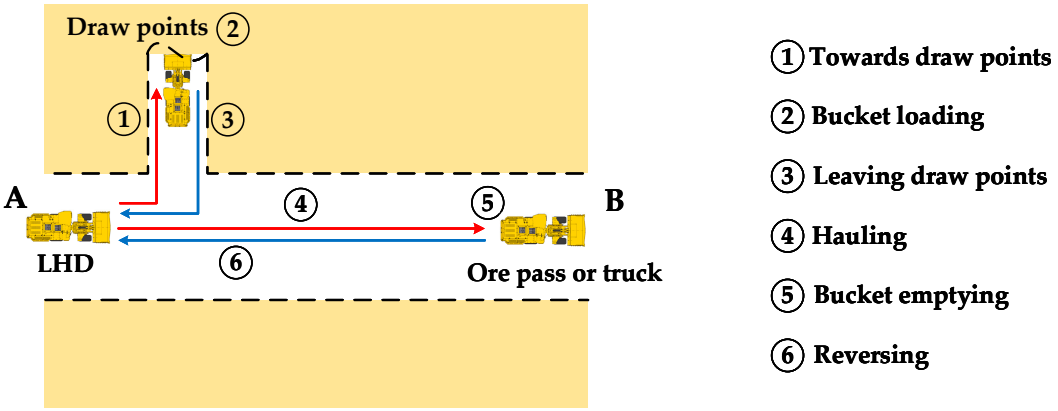

Figure 1. Typical driving cycle of load-haul-dump vehicles (LHDs).

The distance of hauling or the operation sequence may change due to the different working areas and mining tasks; as a result, each driving cycle is not exactly the same. However, for most LHDs, their daily operations are relatively fixed, and will remain constant over a long period of time. Therefore, the driving cycle indicated in Figure 1 can be used as the basis for analyzing the power demand, sizing powertrain parameters, and developing EMS of LHDs.

The data applied in this paper is collected from the underground mine field tests of a 14-ton hybrid electric LHD, as shown in Figure 2, with the road slope of the working area being zero. In order to demonstrate the different characteristics between the traction system and the hydraulic system of an LHD, the curves of traction power and hydraulic power are presented respectively. The speed and power profiles of three driving cycles are illustrated in Figure 3, where the duration is 370 s, the sampling frequency is 1 s, the traction peak power is 204.7 kW, the hydraulic peak power is

82.3 kW, the maximum speed is 7.8 km/h, and the sections with shadow correspond to the bucket loading phases. It can be seen that the power of the traction system is relatively low, except for in the bucket loading phase. This is because, during the bucket loading phase, traction motor needs to supply enough power to drive forward and make the bucket insert into the bottom of the ore heap. While in times of bucket emptying, the LHD only needs to drive to the right point and dump the ore, which requires relatively low power for the traction system. The output of the hydraulic system is mainly in the bucket loading and emptying phases due to the operation of the boom system. The driving speed is slow in the dark, damp, and narrow environment indicated in Figure 2. Therefore, the harsh power profiles of the bucket loading phase make high requirements for the power sources of a LHD.

Figure 2. Underground mine field tests in Anshan, China.

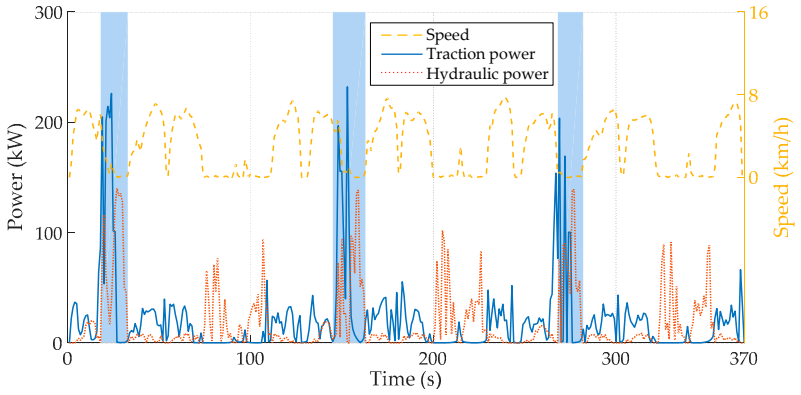

Figure 3. Speed and power profiles of three driving cycles.

3. Powertrain Configuration and Model of a Hybrid ESS Based LHD

3.1. Powertrain Structure

There are several different powertrain topologies in LHD development history. Unlike conventional diesel and hybrid electric LHDs, the powertrain structure with hybrid ESS proposed in this paper eliminates the diesel engine and related accessories powered by lithium-ion BT packs and SC packs. Many configurations of hybrid ESS topology are proposed and compared in different applications. Figure 4 presents the powertrain configuration of the key components of a hybrid ESS-based LHD. First, the use of the bidirectional DC/DC converter behind the SC packs is to allow a wide range of their voltage and to fully utilize their functionalities [41]. Therefore, the SC packs can provide high power instantly when needed. The BT packs are connected directly to the DC bus to keep the voltage stable. Then, the energy on the DC bus is distributed to the traction motor and hydraulic motor via the DC/AC converters, respectively. The traction motor drives the wheels through the axles, and

the hydraulic motor drives the pump to provide energy for the steering, braking, and working systems of the LHD [9]. Besides, the accessories are powered by BT packs via a low-voltage unidirectional DC/DC converter.

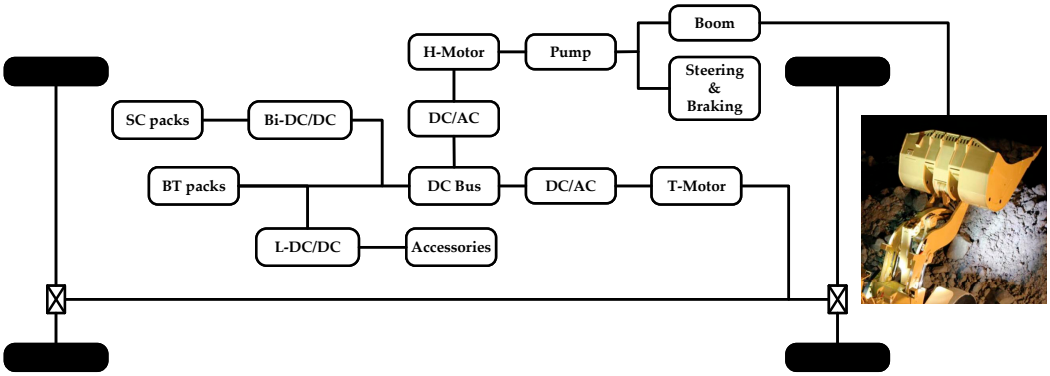

Figure 4. Powertrain configuration of the key components of a hybrid ESS-based LHD.

3.2. Theoretical Model

3.2.1. Battery *Rint* Model

Several papers compare different battery models [44–46]. For the purpose of reducing the computation time, the effects of temperature on the open circuit voltage and the internal resistance are ignored. The *Rint* model [47] of a BT cell, shown in Figure 5a, is adopted to represent the battery behavior.

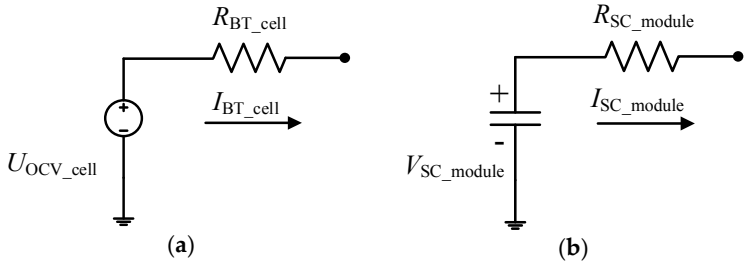

Figure 5. Equivalent circuit models: (**a**) battery (BT) cell; and (**b**) supercapacitor (SC) module.

First of all, from the viewpoint of the BT cell, the current can be calculated as follows:

$$I_{BT\_cell} = \frac{U_{OCV\_cell} - \left(U_{OCV\_cell}^2 - 4 \cdot R_{BT\_cell} \cdot P_{BT\_cell}\right)^{1/2}}{2 \cdot R_{BT\_cell}} \quad (1)$$

where U_{OCV_cell}, P_{BT_cell}, and R_{BT_cell} are the open circuit voltage, the power, and the internal resistance of the BT cell, respectively.

The state of charge (SoC) at the discrete step k ($SoC_{BT\_cell}(k)$) is defined as the current capacity ($Q(k)$) divided by the nominal capacity of the BT cell (Q_{BT_cell}):

$$SoC_{BT\_cell}(k) = Q(k)/Q_{BT\_cell} \cdot 100\% \quad (2)$$

With a timestep of Δt, the SoC at the next step is as follows:

$$SoC_{BT\_cell}(k+1) = SoC_{BT\_cell}(k) - \left(I_{BT\_cell}(k) \cdot \Delta t / Q_{BT\_cell}\right) \cdot 100\% \quad (3)$$

From the perspective of the BT packs, assume that the packs consist of the BT cells mentioned above via N_{BT} series and M_{BT} parallel [22].

$$Q_{BT} = M_{BT} \cdot Q_{BT\_cell} \tag{4}$$

$$R_{BT} = N_{BT} \cdot R_{BT\_cell} / M_{BT} \tag{5}$$

$$V_{BT} = N_{BT} \cdot V_{BT\_cell} \tag{6}$$

where V_{BT_cell} represents the voltage of the BT cell, and Q_{BT}, R_{BT} and V_{BT} represent the nominal capacity, the internal resistance, and the voltage of the BT packs, respectively.

3.2.2. Supercapacitor Model

As with the previous battery modeling method, the SC model is illustrated in Figure 5b. Suppose that the packs are composed of the SC modules via N_{SC} series and M_{SC} parallel [22]:

$$C_{SC} = M_{SC} \cdot C_{SC\_module} / N_{SC} \tag{7}$$

$$R_{SC} = N_{SC} \cdot R_{SC\_module} / M_{SC} \tag{8}$$

$$V_{SC} = V_{SC\_module} \cdot N_{SC} \tag{9}$$

where C_{SC_module}, R_{SC_module} and V_{SC_module} denote the capacity, the internal resistance, and the voltage of the SC module, while C_{SC}, R_{SC} and V_{SC} denote the same meanings of the SC packs.

The relationship between SoC_{SC}, V_{SC}, and stored energy (E_{SC}) of the SC packs can be deduced as follows:

$$SoC_{SC} = V_{SC} / V_{SC\_max} \tag{10}$$

$$E_{SC} = 0.5 \cdot C_{SC} \cdot V_{SC\_max}^2 \cdot (1 - SoC_{SC\_min}^2) \tag{11}$$

where V_{SC_max} and SoC_{SC_min} are the SC packs voltage in a fully charged condition and the lower limit of SC packs voltage. We can conclude that the SC packs can release 75% of its stored energy when the SoC_{SC} drops from 100% to 50% [22]. Therefore, the SoC_{SC_min} is generally set more than 50% from the efficiency perspective. The key parameters of the BT cell and SC module used in this paper are listed in Table 1, which are provided by the manufacturers.

Table 1. Key parameters of the BT cell and SC module.

BT Cell		SC Module	
Nominal voltage (V)	3.3	Nominal voltage (V)	48
Nominal capacity (Ah)	60	Nominal capacity (F)	165
Stored energy (kWh)	0.198	Stored energy (kWh)	0.0528
Internal resistance (mΩ)	1.5	Internal resistance (mΩ)	7.1
Volume (L)	1.15	Volume (L)	14.5

3.2.3. Battery Capacity Degradation Model

The capacity degradation of battery system is defined as a percentage that equals the capacity loss divided by the nominal capacity after a period of operation. Wang et al. [37] developed a cycle-life model including four parameters (time, temperature, depth of discharge, and discharge rate) for the purpose of studying the capacity fade of a $LiFePO_4$ battery, which is shown in Equation (12).

$$Q_{loss} = A \cdot e^{-\left(\frac{E_a + B \cdot C\_Rate}{R \cdot Ten}\right)} (A_h)^z \tag{12}$$

where Q_{loss} is the percentage of capacity loss, A is the pre-exponential factor, E_a is the activation energy in J/mol, R is the gas constant, T_{en} is the absolute temperature in K, A_{h} is the Ah-throughput, C_Rate is the discharge rate, and B is the compensation factor of C_Rate.

Song et al. [22] conducted the degradation experiments on the 3.3 V 60 Ah battery cell. Based on Equation (12) and the experimental data, the battery capacity degradation model was deduced as:

$$Q_{\text{loss}} = 0.0032 \cdot e^{-\left(\frac{15{,}162-1516 \cdot C\_Rate}{R \cdot Ten}\right)} (A_{\text{h}})^{0.824} \tag{13}$$

In this paper, the BT packs consisting of the same battery cell that is illustrated in Table 1 are employed, and Equation (13) is used as the battery capacity degradation model to quantitatively evaluate the capacity loss and the replacement cost.

3.2.4. Other Powertrain Elements

As this study is intended to investigate the energy consumption and the total cost of hybrid ESS, the models of DC/DC converters, traction motor and hydraulic motor are not developed in detail. Assume that the efficiencies of DC/DC converter and motor system are 95% and 93%, respectively, which are the average efficiency values of their operating range [21].

4. Multi-Objective Optimization Problem

4.1. Optimization Framework for Hybrid ESS Parameter Sizing

Productivity is closely related to the daily operation and environment, and depends on several factors, including the number of load/empty runs, bucket capacity, hauling distance, speed, and road slope. Considering that the driving cycle and the bucket capacity are determined in this study, if we can reduce the energy consumption in each driving cycle, working hours will be extended, thereby raising the productivity in the long term. Therefore, energy consumption, as a direct impact on productivity, should be highly valued in the design stage of hybrid ESS-based LHDs.

The performance of the hybrid ESS-based LHD is affected by three aspects: namely, driving cycle, powertrain parameter sizing, and EMS. The pre-defined driving cycle applied in this paper is based on field tests. Consequently, a multi-objective optimization problem that combines parameter sizing and EMS is formulated as follows:

$$\min_{\vec{x}} J = [J_{\text{E}}, J_{\text{C}}] \tag{14}$$

where J is the multi-objective optimization function, J_{E} is the energy consumption in kJ, and J_{C} is the total cost of hybrid ESS in €/day, which will be calculated in detail in Sections 4.2 and 4.3, respectively.

$$\vec{x} = (N_{\text{BT}}, M_{\text{BT}}, N_{\text{SC}}, M_{\text{SC}})^{\text{T}} \in \Omega \tag{15}$$

where $\vec{x}$ is the optimized vector, which involves four variables, including N_{BT}, M_{BT}, N_{SC} and M_{SC}, and Ω is the optimization space, including all parameter vectors in this paper, as shown in Equation (16).

$$\Omega = \left\{ \begin{array}{l} (N_{\text{BT}}, M_{\text{BT}}, N_{\text{SC}}, M_{\text{SC}}) | N_{\text{BT}} \in \{170, 172, 174, \cdots, 200\}, \\ M_{\text{BT}} \in \{6, 7, 8\}, \\ N_{\text{SC}} \in \{11, 12, 13, 14, 15\}, M_{\text{SC}} \in \{1\} \end{array} \right\} \tag{16}$$

where the BT series changes between 170 and 200, and the corresponding lower and upper nominal voltage limits of BT packs are 561 V and 660 V, which belong to the working range of DC/AC converters (400~720 V), the BT parallel varies from 6 to 8 in order to satisfy at least six hours of working time, the SC series changes between 11 and 15 to guarantee the output power can meet the harsh requirements, and in consideration of the space constraints and stored energy of the SC packs, the number of SC parallel is 1.

The two optimization objectives defined in Equation (14), which relate to energy consumption and the total cost of hybrid ESS, have different physical meanings, and are difficult to evaluate in one equation. However, we can use a method based on Pareto optimization to solve the problem mentioned above [48].

Figure 6 illustrates a multi-objective optimization framework with a DP-based EMS and a life cycle cost model of hybrid ESS to obtain the Pareto optimal solution. First of all, a parameter vector $\vec{x}$ is selected from the optimization space as the variable of multi-objective optimization. Through the function J, $\vec{x}$ is used as the inputs of EMS and the life cycle cost model. DP-based EMS is then conducted to calculate the minimal energy consumption $J_{\mathrm{E}}(\vec{x})$, and to find the optimal BT packs current profile $I_{\mathrm{BT}}(t)$, which is used to achieve the battery capacity loss Q_{loss}. After that, the total cost of hybrid ESS $J_{\mathrm{C}}(\vec{x})$ is gained using the Q_{loss} and the cost model. Each $\vec{x}$ repeats the same procedure as mentioned above. Finally, all $(J_{\mathrm{E}}, J_{\mathrm{C}})$ are compared and evaluated to find an acceptable energy consumption and total cost as the Pareto optimal solution.

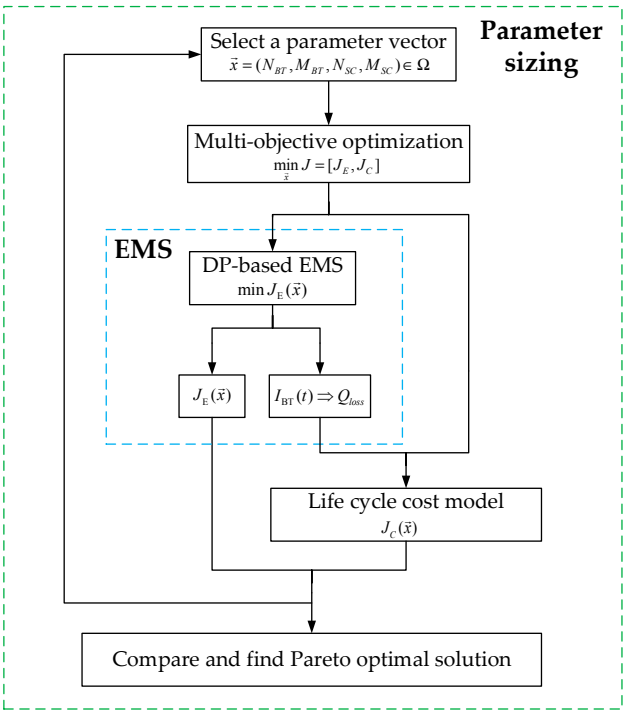

Figure 6. Structure of the multi-objective optimization framework.

4.2. DP-Based Energy Management Strategy

The DP is a discrete global optimization algorithm that is widely applied to solve the problem of energy management strategy of hybrid ESS-based vehicles [11,49–52]. In terms of the design stage of the LHD, we need to use the method of DP to obtain the optimal solution for the hybrid ESS-based optimization problem, and to evaluate the other results based on this benchmark. This paper employs the DP algorithm implemented by Song et al. [11] to minimize the energy consumption of a hybrid ESS-based LHD, with an objective function and constraints as follows:

$$\min J_{\mathrm{E}}(\vec{x}) = \sum_{k=1}^{T-1} (E_{\mathrm{BT}}(k) + E_{\mathrm{SC}}(k)) + E_{\mathrm{BT}}(k+1) + E_{\mathrm{SC}}(k+1) \tag{17}$$

$$s.t.\begin{cases} P_{\text{dem}}(k) = P_{\text{cycle}}(k), k \in [0, T-1] \\ SoC_{\text{SC}} \in [SoC_{\text{SC\_L}}, SoC_{\text{SC\_H}}] \\ SoC_{\text{SC\_0}} = SoC_{\text{SC\_end}} \\ I_{\text{BT}} \in [0, I_{\text{BT\_max}}] \\ P_{\text{SC}} \in [P_{\text{SC\_min}}, P_{\text{SC\_max}}] \end{cases} \tag{18}$$

where P_{dem} is the power demand, P_{cycle} is the total power of the driving cycle, and T is the number of sample points for the driving cycle and normally, the discrete step is 1 s. $SoC_{\text{SC\_L}}$ and $SoC_{\text{SC\_H}}$ are the lower and upper limits of the SoC_{SC}, $SoC_{\text{SC\_0}}$ is the initial SoC value, $SoC_{\text{SC\_end}}$ is the end SoC value, $P_{\text{SC\_min}}$ and $P_{\text{SC\_max}}$ are the minimal and maximal power of the SC packs, $I_{\text{BT\_max}}$ is the maximal discharge current of the BT packs.

The power released from hybrid ESS needs to satisfy the power demand of the driving cycle shown in Equation (19), where P_{BT} and P_{SC} represent the actual output power of the BT and SC packs after considering the efficiency of the DC/DC converter.

$$P_{\text{dem}}(k) = P_{\text{BT}}(k) + P_{\text{SC}}(k) \tag{19}$$

Consider the voltage V_{SC} and the voltage change ΔV_{SC} of SC packs as the state and decision variables, respectively, and the interval of V_{SC} is 0.2 V. In Equation (20), $\Delta V_{\text{SC}}(k, k-1)$ represents the voltage change of SC packs from sample time $k-1$ to k. The energy consumption of the BT and SC packs are described in Equations (21) and (22).

$$V_{\text{SC}}(k) = V_{\text{SC}}(k-1) + \Delta V_{\text{SC}}(k, k-1) \tag{20}$$

$$E_{\text{SC}}(k) = 0.5 \cdot C_{\text{SC}} \cdot (V_{\text{SC}}^2(k) - V_{\text{SC}}^2(k-1)) \tag{21}$$

$$E_{\text{BT}}(k) = P_{\text{BT}}(k) \cdot \Delta t(k) \tag{22}$$

Due to the linear relationship between V_{SC} and SoC_{SC}, which is depicted in Equation (10), we use SoC_{SC} to replace V_{SC} during the process of the DP algorithm illustrated in Figure 7.

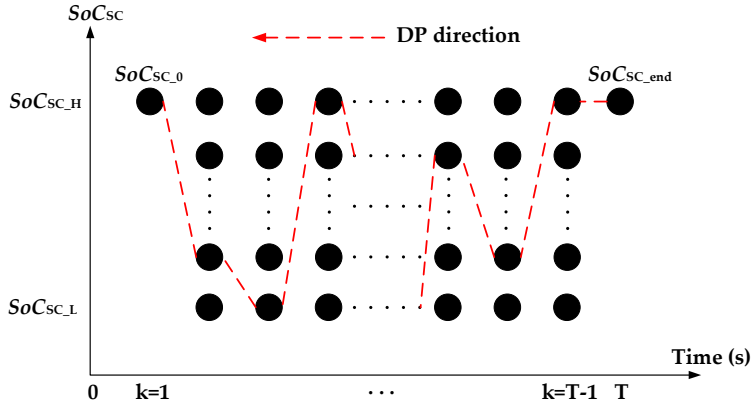

Figure 7. Process of the dynamic programming (DP) algorithm.

In this paper, the energy stored in the BT packs can be used for at least six hours. However, the duration of the driving cycle is 370 s, and the energy consumption is very low when compared to six hours of working time. Therefore, we do not set the lower limit of the BT packs and assume that the initial SoC of BT packs is 90%. Table 2 presents all the parameters for the DP algorithm. In order to fully utilize the SC packs, we set the lower and upper limits of the SoC at 50% and 100%, the initial SoC of SC packs at 100%, and the peak power of charge and discharge at −250 kW and 250 kW to meet the power and energy requirements. Besides, the maximum current of the BT packs is set to

0.5 C to protect their lifetime. Then, the DP algorithm can be solved step-by-step from the end to the start of the driving cycle. As a result, the optimal energy consumption and hybrid ESS profiles of each parameter vector $\vec{x}$ are obtained.

Table 2. Parameters for the DP algorithm.

Coefficient	Value	Unit
T	370	s
SoC_{SC_L}	50	%
SoC_{SC_H}	100	%
$SoC_{SC\_0}(SoC_{SC\_end})$	100	%
P_{SC_min}	−250	kW
P_{SC_max}	250	kW
I_{BT_max}	0.5 C [1]	A

[1] Discharge rate of the battery.

4.3. Life Cycle Cost Model of Hybrid ESS

In order to consider the total cost of a hybrid ESS for LHDs, a life cycle cost model is established. J_C consists of three parts: the capital costs of BT packs, SC packs, and DC/DC converters $Cost_{cap}$ in €/year; the operating cost of electricity $Cost_{ope}$ in €/day; and the replacement cost $Cost_{rep}$ of the BT packs in €/year, and is illustrated in Equation (23). According to the continuous operations of the LHD, we assume that it works 24 h a day and 360 days a year. The expressions of $Cost_{cap}$ are calculated as Equations (24)–(28).

$$J_C(\vec{x}) = Cost_{cap}/360 + Cost_{ope} + Cost_{rep}/360 \tag{23}$$

$$Cost_{cap} = (BT_{cap} + SC_{cap} + DC_{cap}) \cdot CRF \tag{24}$$

$$BT_{cap} = C_{kWh\_BT} \cdot N_{BT} \cdot M_{BT} \cdot E_{BT\_cell} \tag{25}$$

$$SC_{cap} = C_{kWh\_SC} \cdot N_{SC} \cdot M_{SC} \cdot E_{SC\_cell} \tag{26}$$

$$DC_{cap} = C_{kW\_DC} \cdot (P_{ACC} + P_{SC\_max}) \tag{27}$$

$$CRF = \frac{i \cdot (1+i)^{RT}}{(1+i)^{RT} - 1} \tag{28}$$

where BT_{cap}, SC_{cap}, and DC_{cap} are the capital costs of BT packs, SC packs, and DC/DC converters in €, C_{kWh_BT} and C_{kWh_SC} are the referential costs of BT and SC packs in €/kWh, C_{kW_DC} is the referential cost of DC/DC converters in €/kW, P_{ACC} is the nominal power of the accessories in kW, and CRF is the capital recovery factor, depending on the interest rate i and the reference time RT [53].

$$Cost_{ope} = (E_{BT} + E_{SC}) \cdot C_{kWh\_e}/T \cdot 3600 \times 24 \cdot U \tag{29}$$

where C_{kWh_e} is the reference cost of electricity in €/kWh, and U is the mean utilization of LHDs.

$$Q_{loss\_y} = Q_{loss}/T \cdot 3600 \times 24 \times 360 \cdot U \cdot RT \tag{30}$$

where Q_{loss_y} represents the battery capacity loss within the reference time and the battery packs that need to be replaced when the loss exceeds 20%. In Equations (29) and (30), the duration of the driving cycle T is used to convert the unit to seconds and then multiply the corresponding coefficients to obtain the results.

$$n\_BT = ceil(Q_{loss\_y}/0.2 - 1) \tag{31}$$

$$Cost_{rep} = \sum_{n=1}^{n\_BT} (1+i)^{-n \cdot 0.2} \cdot BT_{cap} \cdot CRF \tag{32}$$

where *n_BT* is the number of BT replacements during the reference time, *ceil*( ) is the function obtaining the higher integer value of its argument. The replacement cost can be deduced in Equation (32). All the parameters for the life cycle cost model are defined in Table 3. In addition to those parameters cited from other references, we assume that the absolute temperature of the working area is 303.15 K and the nominal power of accessories is 5 kW.

Table 3. Parameters for the life cycle cost model.

Coefficient	Value	Unit
C_{kWh_BT}	500 [21]	€/kWh
C_{kWh_SC}	4000 [21]	€/kWh
C_{kW_DC}	150 [21]	€/kW
C_{kWh_e}	0.05 [53]	€/kWh
i	2.5 [53]	%
U	60 [1]	%
RT	10 [1]	Years
T_{en}	303.15	K
P_{ACC}	5	kW

4.4. Pareto Optimal Solution

There are 240 solutions calculated by the DP algorithm and cost model. Figure 8 presents the multi-objective optimization results, showing the relationship between energy consumption and total cost of hybrid ESS. The points in three colors represent the parameter vectors where M_{BT} is 6, 7, and 8, respectively. It could be realized that the energy consumption can be reduced when the total cost of hybrid ESS is increased, because with the increase in the number of hybrid ESS, the peak power of each cell or module will be lower and the efficiency will be improved. The energy consumption of all of the vectors moves within the range of 1.63×10^4 kJ and 1.71×10^4 kJ, while the total cost of hybrid ESS ranges from 150 €/day to 270 €/day.

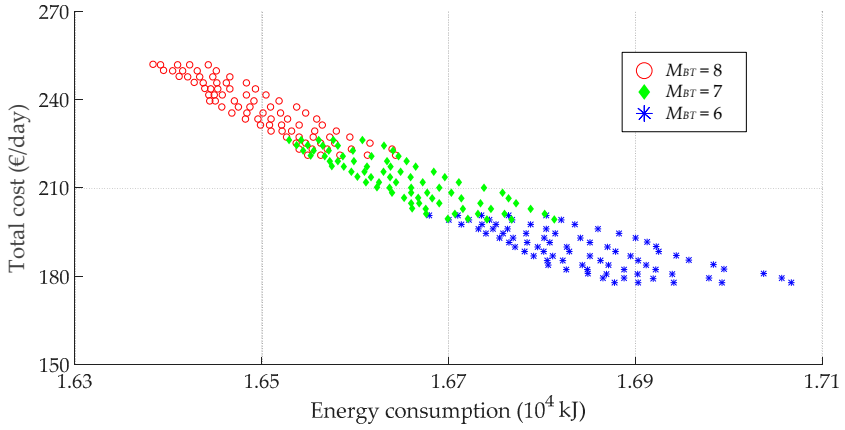

Figure 8. Multi-objective optimization results.

In order to further illustrate the distribution of each vector, taking $M_{BT} = 8$ as an example, 80 solutions are shown in Figure 9. Each blue line stands for a different value of N_{BT}, which is marked on the right side of the line. According to the calculation results, five points from right to left on the same line represent the N_{SC} from 11 to 15, respectively, and the difference in total cost among these points is very small. This distribution explained above also applies to the situations where $M_{BT} = 7$ and $M_{BT} = 6$.

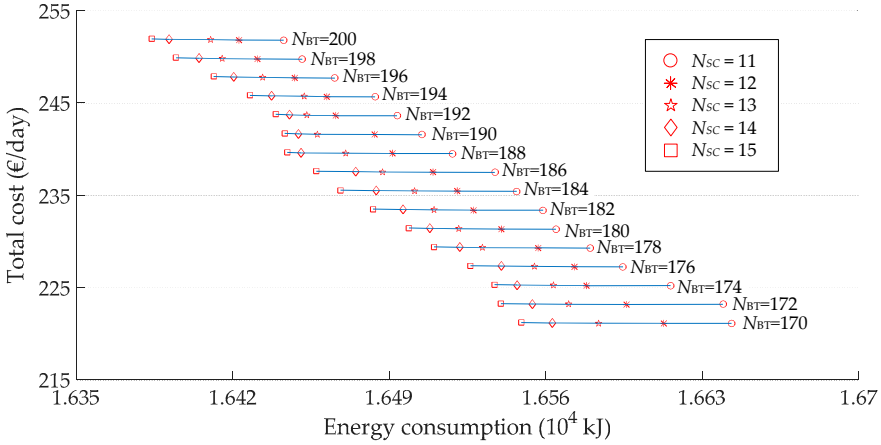

Figure 9. Distribution of the parameter vectors when $M_{BT} = 8$.

In general, any solution in the Pareto front can be considered as the optimal solution from different points of view. The Pareto front solutions in this paper are illustrated in Figure 10. The left boundary in blue line is the Pareto front, which consists of 48 different Pareto solutions. By moving along the front, we could minimize the total cost at the expense of energy consumption, or minimize energy consumption at the expense of total cost, but cannot improve both at once. Compared with Figure 8, we have retained 48 of 240 solutions near the minimum value of both axes, and eliminated the others away from the Pareto front due to their unsatisfactory values. According to the distribution described in Figure 9, it can be seen that all of the $N_{SC} = 15$ situations, that is, the leftmost points of each line, are the Pareto front solutions. We have proposed three optimal solutions selected from the Pareto front. These solutions in Figure 10 include the hybrid ESS with the least energy consumption #1, least total cost #3, and #2, which reflects the trade-off relationship between the two optimization objectives. Table 4 illustrates the values of optimization variables, objectives, and key parameters for the chosen solutions, where N_{SC} and M_{SC} are the same, and all belong to the three-replacement case. The energy consumption varies from 1.639×10^4 kJ to 1.707×10^4 kJ. The total cost and volume of the hybrid ESS is from 177.92 €/day to 251.95 €/day and 1333 L to 2058 L, respectively.

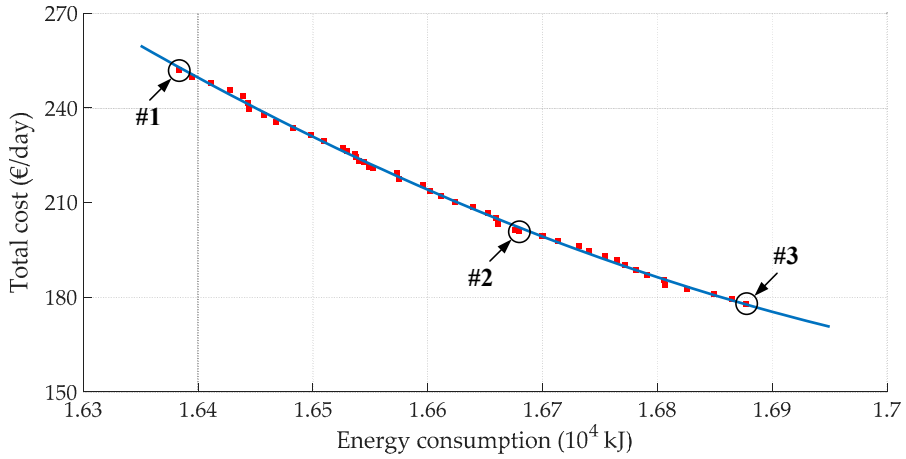

Figure 10. Pareto front solutions.

Table 4. Optimal solutions in the Pareto front.

Solution	N_{BT}	M_{BT}	N_{SC}	M_{SC}	J_E (10^4 kJ)	Q_{loss_y} (%)	J_C (€/Day)	The Volume of Hybrid ESS (L)
#1	200	8	15	1	1.639	60.214	251.95	2058
#2	200	6	15	1	1.668	63.100	200.74	1598
#3	170	6	15	1	1.707	75.234	177.92	1333

The simulation results of the selected solutions, as shown in Figure 11, illustrate the differences among the total cost and proportion of the hybrid ESS, and the SC and BT packs' output profiles. As evidenced from Figure 11a, the sum of BT replacement and capital costs of each solution has reached over 71.6% of the total cost of the hybrid ESS, and even the ratio in #1 is 79.3%. Therefore, it is very important to consider the battery capacity degradation when studying how to reduce the total cost of a hybrid ESS. The battery current becomes more stable by adding supercapacitors into the ESS, which extend battery life. The more supercapacitors used in the solution, the battery current is smaller, as indicated in Figure 11b. Figure 11c,d shows that the SC packs release a lot of energy during the bucket loading phase and could be recharged by BT packs in other phases. The SC packs in #3 operate in a wider range when compared with #1 and #2, which means it is more efficient.

In summary, solution #2 ($N_{BT} = 200$, $M_{BT} = 6$, $N_{SC} = 15$ and $M_{SC} = 1$) can not only balance the relationship between the two objectives well, it also shows the desirable effects on the aspects of BT and SC pack profiles. Besides, 200 series and six parallel BT cells would be more appropriate for grouping, and can save a lot of space on the hybrid ESS-based LHD. Therefore, solution #2 is selected as the Pareto optimal solution in this paper.

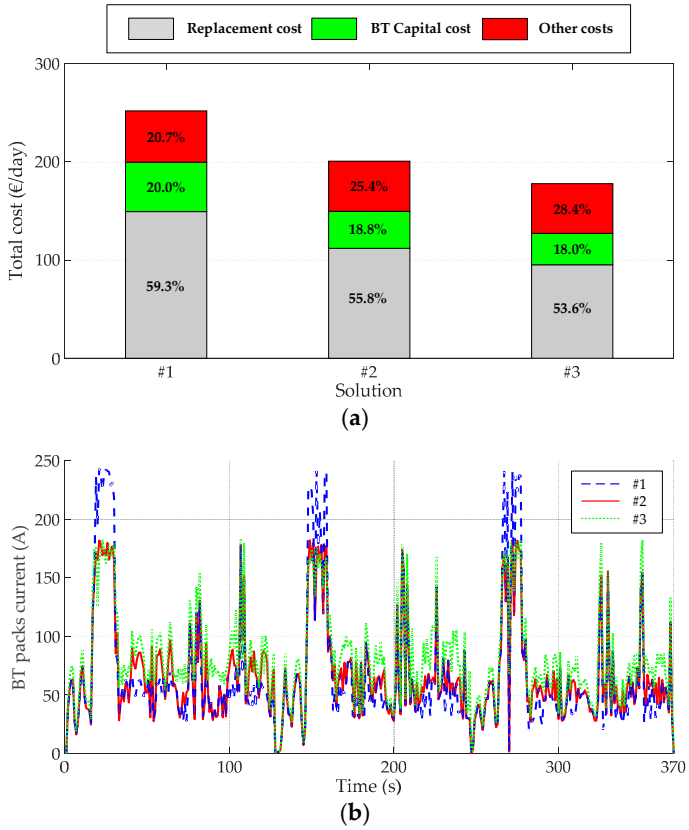

Figure 11. *Cont.*

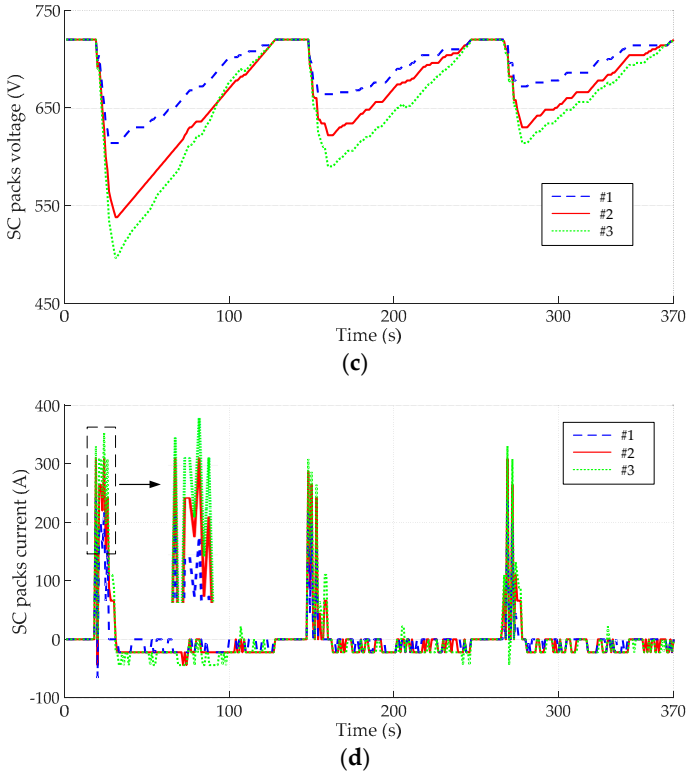

Figure 11. Selected solutions in the Pareto front: (**a**) Total cost and proportion of a hybrid energy storage system (ESS); (**b**) BT packs current; (**c**) SC packs voltage; and (**d**) SC packs current.

5. Comparison with Battery-Only Option

The battery, as the only power source on underground LHDs, must provide enough power to meet the harsh requirements of daily operation. As can be seen in Section 2, the power demand of LHDs varies instantaneously. So, the battery system needs to operate in frequent discharge conditions, which tends to have undesirable effects on battery lifetime. In order to quantitatively compare the performance for both Pareto optimal (hybrid ESS #2) and battery-only options, the BT packs' current is illustrated in Figure 12a. It can be observed that the peak current of the battery-only option reaches 534 A, while the one of the optimal option is only 183 A. The absence of SC packs causes a more transient and higher battery current for the battery-only ESS. Also, the battery capacity loss trajectory is presented in Figure 12b, which indicates that the BT packs in the hybrid ESS are protected more effectively. Besides, calculation results for both the optimal and battery-only options are listed in Table 5. It is obvious that the battery-only ESS is a more expensive option, although its capital cost is relatively low. It can also be noticed that the higher battery capacity loss leads to an increased replacement cost. Furthermore, the optimal ESS is a more efficient option with less energy consumption.

It can be concluded that the hybrid ESS-based LHDs show a better performance in both J_E and J_C when compared with battery-only ones. However, the differences in the performance of both options are very small. The main reason, in the author's opinion, could be the driving cycle. The driving cycle of the LHD only has traction mode and does not include regenerative braking mode. This means that the frequent braking during the driving cycle will not be considered. On the one hand, if the braking energy is not recovered, it will not fully utilize the functionalities of the SC packs, which inevitably leads to a decrease in the overall efficiency of the hybrid ESS option. On the other hand, if the regenerative braking mode is added, the energy will be directly recovered into the BT packs of the battery-only option, and the high-frequency charge current will definitely exacerbate the battery

capacity loss, thereby increasing the total cost. Thus, it is necessary to consider regenerative braking mode for further study.

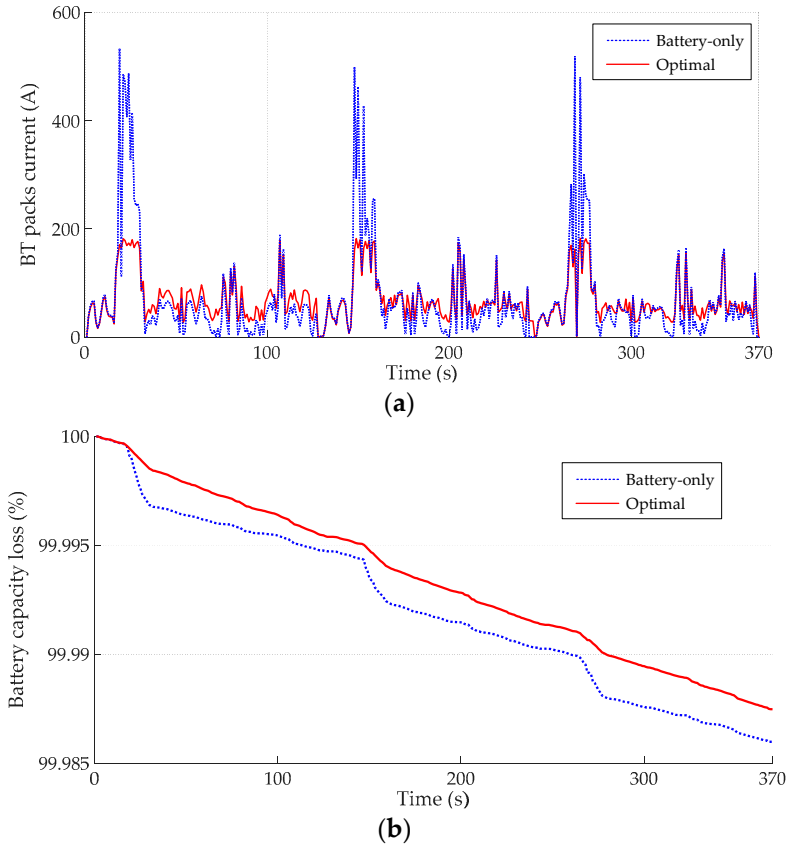

Figure 12. Comparison between the optimal and battery-only options: (**a**) BT packs current; and (**b**) Battery capacity loss trajectory.

Table 5. Calculation results for both optimal and battery-only options.

Option	Hybrid ESS Capital Cost (€/Day)	Battery Loss during 370 s (10^{-4}%)	Replacement Cost (€/Day)	J_E (10^4 kJ)	J_C (€/Day)
Optimal	50.62	1.25	112.01	1.668	200.74
Battery-only	37.71	1.41	129.24	1.679	204.15

6. Conclusions

This paper proposes a multi-objective optimization problem of parameter sizing for a hybrid ESS-based LHD regarding energy consumption and the total cost of a hybrid ESS, and a battery capacity degradation model is used. In order to enhance the overall performance, a hybrid ESS-based powertrain configuration is presented to satisfy the harsh requirements of the driving cycle. In the optimization framework, taking sizes of both the BT and SC packs as variables, DP-based EMS and Pareto optimization are employed, with a life cycle cost model established in the context. The Pareto optimal hybrid ESS and battery-only options are compared quantitatively at last.

The important findings are summarized below:

- The sum of BT replacement and capital costs has reached over 71.6% of the total cost of hybrid ESS, which highlights the importance of considering the battery capacity degradation when evaluating the total cost of hybrid ESS-based LHDs.

- As the total cost of hybrid ESS increases, the energy consumption becomes smaller. Three solutions chosen from the Pareto front are compared comprehensively, and #2 ($N_{BT} = 200$, $M_{BT} = 6$, $N_{SC} = 15$ and $M_{SC} = 1$) is selected as the Pareto optimal solution, which can make an ideal trade-off between the two objectives, where the energy consumption and the total cost is 1.668×10^4 kJ and 200.74 €/day, respectively.
- Comparison with battery-only option indicates that the optimal hybrid ESS is a more economical and efficient option.

Acknowledgments: This work was supported by the Beijing Excellent Talent Training Program in 2015, the National Key Research and Development Program under Project No. 2016YFC0802905 and National Natural Science Foundation of China, No. 51276012.

Author Contributions: Jiajun Liu and Tianxu Jin conceived and designed the simulations; Li Liu, Yajue Chen and Kun Yuan analyzed the data; Jiajun Liu wrote the paper.

Conflicts of Interest: The authors declare no conflict of interest.

References

1. Jacobs, W.; Hodkiewicz, M.; Bräunl, T. A Cost-Benefit Analysis of Electric Loaders to Reduce Diesel Emissions in Underground Hard Rock Mines. *IEEE Trans. Ind. Electron.* **2015**, *51*, 2565–2573. [CrossRef]
2. Luo, X.; Wang, J.; Dooner, M.; Clarke, J. Overview of current development in electrical energy storage technologies and the application potential in power system operation. *Appl. Energy* **2015**, *137*, 511–536. [CrossRef]
3. Lajunen, A.; Suomela, J. Evaluation of energy storage system requirements for hybrid mining loaders. *IEEE Trans. Veh. Technol.* **2012**, *61*, 3387–3393. [CrossRef]
4. Zeng, X.; Yang, N.; Peng, Y.; Zhang, Y.; Wang, J. Research on energy saving control strategy of parallel hybrid loader. *Autom. Constr.* **2014**, *38*, 100–108. [CrossRef]
5. Nilsson, T.; Fröberg, A.; Åslund, J. Predictive control of a diesel electric wheel loader powertrain. *Control Eng. Pract.* **2015**, *41*, 47–56. [CrossRef]
6. Kwon, T.; Lee, S.; Sul, S.; Park, C.; Kim, N.; Kang, B.; Hong, M. Power Control Algorithm for Hybrid Excavator with Supercapacitor. *IEEE Trans. Ind. Appl.* **2010**, *46*, 1447–1455. [CrossRef]
7. Wang, D.; Guan, C.; Pan, S.; Zhang, M.; Lin, X. Performance analysis of hydraulic excavator powertrain hybridization. *Autom. Constr.* **2009**, *18*, 249–257. [CrossRef]
8. Unger, J.; Kozek, M.; Jakubek, S. Nonlinear model predictive energy management controller with load and cycle prediction for non-road HEV. *Control Eng. Pract.* **2015**, *36*, 120–132. [CrossRef]
9. Yoon, J.; Truong, D.; Ahn, K. A generation step for an electric excavator with a control strategy and verifications of energy consumption. *Int. J. Precis. Eng. Manuf.* **2013**, *14*, 755–766. [CrossRef]
10. Kim, M.; Peng, H. Power management and design optimization of fuel cell/battery hybrid vehicles. *J. Power Sour.* **2007**, *165*, 819–832. [CrossRef]
11. Song, Z.; Hofmann, H.; Li, J.; Han, X.; Ouyang, M. Optimization for a hybrid energy storage system in electric vehicles using dynamic programing approach. *Appl. Energy* **2015**, *139*, 151–162. [CrossRef]
12. Song, Z.; Hou, J.; Xu, S.; Ouyang, M.; Li, J. The influence of driving cycle characteristics on the integrated optimization of hybrid energy storage system for electric city buses. *Energy* **2017**, *135*, 91–100. [CrossRef]
13. Hung, Y.; Wu, C. A combined optimal sizing and energy management approach for hybrid in-wheel motors of EVs. *Appl. Energy* **2015**, *139*, 260–271. [CrossRef]
14. Liu, C.; Liu, L. Optimal power source sizing of fuel cell hybrid vehicles based on Pontryagin's minimum principle. *Int. J. Hydrog. Energy* **2015**, *40*, 8454–8464. [CrossRef]
15. Murgovski, N.; Johannesson, L.; Sjöberg, J.; Egardt, B. Component sizing of a plug-in hybrid electric powertrain via convex optimization. *Mechatronics* **2012**, *22*, 106–120. [CrossRef]
16. Hu, X.; Johannesson, L.; Murgovski, N.; Egardt, B. Longevity-conscious dimensioning and power management of the hybrid energy storage system in a fuel cell hybrid electric bus. *Appl. Energy* **2015**, *137*, 913–924. [CrossRef]

17. Hu, X.; Moura, S.; Murgovski, N.; Egardt, B.; Cao, D. Integrated Optimization of Battery Sizing, Charging, and Power Management in Plug-In Hybrid Electric Vehicles. *IEEE Trans. Control Syst. Technol.* **2016**, *24*, 1036–1043. [CrossRef]
18. Hu, X.; Jiang, J.; Egardt, B.; Cao, D. Advanced power-source integration in hybrid electric vehicles: Multicriteria optimization approach. *IEEE Trans. Ind. Electron.* **2015**, *62*, 7847–7858. [CrossRef]
19. Xu, L.; Mueller, C.; Li, J.; Ouyang, M.; Hu, Z. Multi-objective component sizing based on optimal energy management strategy of fuel cell electric vehicles. *Appl. Energy* **2015**, *157*, 664–674. [CrossRef]
20. Ebbesen, S.; Dönitz, C.; Guzzella, L. Particle swarm optimization for hybrid electric drive-train sizing. *Int. J. Veh. Des.* **2012**, *58*, 181–199. [CrossRef]
21. Herrera, V.; Milo, A.; Gaztañaga, H.; Otadui, I.; Villarreal, I.; Camblong, H. Adaptive energy management strategy and optimal sizing applied on a battery-supercapacitor based tramway. *Appl. Energy* **2016**, *169*, 831–845. [CrossRef]
22. Song, Z.; Li, J.; Han, X.; Xu, L.; Lu, L.; Ouyang, M.; Hofmann, H. Multi-objective optimization of a semi-active battery/supercapacitor energy storage system for electric vehicles. *Appl. Energy* **2014**, *135*, 212–224. [CrossRef]
23. Hu, Z.; Li, J.; Xu, L.; Song, Z.; Fang, C.; Ouyang, M.; Dou, G.; Kou, G. Multi-objective energy management optimization and parameter sizing for proton exchange membrane hybrid fuel cell vehicles. *Energy Convers. Manag.* **2016**, *129*, 108–121. [CrossRef]
24. Martinez, C.; Hu, X.; Cao, D.; Velenis, E.; Gao, B.; Wellers, M. Energy management in plug-in hybrid electric vehicles: Recent progress and a connected vehicles perspective. *IEEE Trans. Veh. Technol.* **2017**, *66*, 4534–4549. [CrossRef]
25. Silvas, E.; Hofman, T.; Murgovski, N.; Etman, L.; Steinbuch, M. Review of optimization strategies for system-level design in hybrid electric vehicles. *IEEE Trans. Veh. Technol.* **2017**, *66*, 57–70. [CrossRef]
26. Zhang, W.; Li, J.; Xu, L.; Ouyang, M. Optimization for a fuel cell/battery/capacity tram with equivalent consumption minimization strategy. *Energy Convers. Manag.* **2017**, *134*, 59–69. [CrossRef]
27. Hemi, H.; Ghouili, J.; Cheriti, A. Combination of Markov chain and optimal control solved by Pontryagin's Minimum Principle for a fuel cell/supercapacitor vehicle. *Energy Convers. Manag.* **2015**, *91*, 387–393. [CrossRef]
28. Wieczorek, M.; Lewandowski, M. A mathematical representation of an energy management strategy for hybrid energy storage system in electric vehicle and real time optimization using a genetic algorithm. *Appl. Energy* **2017**, *192*, 222–233. [CrossRef]
29. Scooptram ST7 Battery. Available online: https://www.atlascopco.com/en-cn/mrba/products/loaders-and-trucks/electric-loaders/scooptram-st7-battery (accessed on 7 July 2017).
30. MUCKMASTER 300EB. Available online: http://www.rdhminingequipment.com/product/muckmaster-300eb/ (accessed on 12 July 2017).
31. MUCKMASTER 600EB. Available online: http://www.rdhminingequipment.com/product/muckmaster-600eb/ (accessed on 12 July 2017).
32. 153-Artisan Vehicle Systems. Available online: http://artisanvs.com/project/153/ (accessed on 13 July 2017).
33. Catherino, H.; Burgel, J.; Shi, P.; Rusek, A.; Zou, X. Hybrid power supplies: A capacitor-assisted battery. *J. Power Sour.* **2006**, *162*, 965–970. [CrossRef]
34. Pagano, M.; Piegari, L. Hybrid electrochemical power sources for onboard applications. *IEEE Trans. Energy Convers.* **2007**, *22*, 450–456. [CrossRef]
35. Lu, S.; Corzine, K.; Ferdowsi, M. A new battery/ultracapacitor energy storage system design and its motor drive integration for hybrid electric vehicles. *IEEE Trans. Veh. Technol.* **2007**, *56*, 1516–1523. [CrossRef]
36. Schaltz, E.; Khaligh, A.; Rasmussen, P. Influence of battery/ultracapacitor energy-storage sizing on battery lifetime in a fuel cell hybrid electric vehicle. *IEEE Trans. Veh. Technol.* **2009**, *58*, 3882–3891. [CrossRef]
37. Wang, J.; Liu, P.; Garner, J.; Sherman, E.; Soukiazian, S.; Verbrugge, M.; Tataria, H.; Musser, J.; Finamore, P. Cycle-life model for graphite-$LiFePO_4$ cells. *J. Power Sour.* **2011**, *196*, 3942–3948. [CrossRef]
38. Ouyang, M.; Feng, X.; Han, X.; Lu, L.; Li, Z.; He, X. A dynamic capacity degradation model and its applications considering varying load for a large format Li-ion battery. *Appl. Energy* **2016**, *165*, 48–59. [CrossRef]
39. Cericola, D.; Ruch, P.; Kötz, R.; Novák, P.; Wokaun, A. Simulation of a supercapacitor/Li-ion battery hybrid for pulsed applications. *J. Power Sour.* **2010**, *195*, 2731–2736. [CrossRef]

40. Trovão, J.; Pereirinha, P.; Jorge, H.; Antunes, C. A multi-level energy management system for multi-source electric vehicles-An integrated rule-based meta-heuristic approach. *Appl. Energy* **2013**, *105*, 304–318. [CrossRef]
41. Hung, Y.; Wu, C. An integrated optimization approach for a hybrid energy system in electric vehicles. *Appl. Energy* **2012**, *98*, 479–490. [CrossRef]
42. Cao, J.; Emadi, A. A new battery/ultracapacitor hybrid energy storage system for electric, hybrid, and plug-in hybrid electric vehicles. *IEEE Trans. Power Electron.* **2012**, *27*, 122–132. [CrossRef]
43. Wang, Y.; Wang, W.; Zhao, Y.; Yang, L.; Chen, W. A Fuzzy-Logic Power Management Strategy Based on Markov Random Prediction for Hybrid Energy Storage Systems. *Energies* **2016**, *9*, 25. [CrossRef]
44. Hu, X.; Li, S.; Peng, H. A comparative study of equivalent circuit models for Li-ion batteries. *J. Power Sour.* **2012**, *198*, 359–367. [CrossRef]
45. He, H.; Xiong, R.; Guo, H.; Li, S. Comparison study on the battery models used for the energy management of batteries in electric vehicles. *Energy Convers. Manag.* **2012**, *64*, 113–121. [CrossRef]
46. Einhorn, M.; Conte, F.; Kral, C.; Fleig, J. Comparison, selection, and parameterization of electrical battery models for automotive applications. *IEEE Trans. Power Electron.* **2013**, *28*, 1429–1437. [CrossRef]
47. Plett, G. Extended Kalman filtering for battery management systems of LiPB-based HEV battery packs Part 2. Modeling and identification. *J. Power Sour.* **2004**, *134*, 262–276. [CrossRef]
48. Marler, R.; Arora, J. Survey of multi-objective optimization methods for engineering. *Struct. Multidiscip. Optim.* **2004**, *26*, 369–395. [CrossRef]
49. Ansarey, M.; Panahi, M.; Ziarati, H.; Mahjoob, M. Optimal energy management in a dual-storage fuel-cell hybrid vehicle using multi-dimensional dynamic programming. *J. Power Sour.* **2014**, *250*, 359–371. [CrossRef]
50. Santucci, A.; Sorniotti, A.; Lekakou, C. Power split strategies for hybrid energy storage systems for vehicular applications. *J. Power Sour.* **2014**, *258*, 395–407. [CrossRef]
51. Pérez, L.; Bossio, G.; Moitre, D.; García, G. Optimization of power management in an hybrid electric vehicle using dynamic programming. *Math. Comput. Simul.* **2006**, *73*, 244–254. [CrossRef]
52. Xu, L.; Yang, F.; Li, J.; Ouyang, M.; Hua, J. Real time optimal energy management strategy targeting at minimizing daily operation cost for a plug-in fuel cell city bus. *Int. J. Hydrogen Energy* **2012**, *37*, 15380–15392. [CrossRef]
53. Zakeri, B.; Syri, S. Electrical energy storage systems: A comparative life cycle cost analysis. *Renew. Sustain. Energy Rev.* **2015**, *42*, 569–596. [CrossRef]